



ELSEVIER

Available online at [www.sciencedirect.com](http://www.sciencedirect.com)

SCIENCE @ DIRECT®

Optics Communications 251 (2005) 165–171

OPTICS  
COMMUNICATIONS

[www.elsevier.com/locate/optcom](http://www.elsevier.com/locate/optcom)

## Multiconical emission of a monolithic mini-cavity optical parametric oscillator

Martynas Peckus<sup>a,\*</sup>, Kestutis Staliunas<sup>b</sup>, Mark Saffman<sup>c</sup>, Gintas Slekyš<sup>d</sup>,  
Valdas Sirutkaitis<sup>a</sup>, Valerijus Smilgevicius<sup>a</sup>, Rimantas Grigonis<sup>a</sup>

<sup>a</sup> *Laser Research Center, Department of Quantum Electronics, Vilnius University, Sauletekio Avenue 10, 10223 Vilnius, Lithuania*

<sup>b</sup> *ICREA, Departament de Física i Enginyeria Nuclear, Universitat Politècnica de Catalunya, Colom 11, E-08222 Terrassa, Barcelona, Spain*

<sup>c</sup> *Department of Physics, 1150 University Avenue, University of Wisconsin, Madison, WI 53706, USA*

<sup>d</sup> *Altechna, Vilnius, Lithuania*

Received 26 November 2004; received in revised form 15 February 2005; accepted 17 February 2005

### Abstract

We show experimentally, and interpret theoretically the conical and multiconical emission of degenerate optical parametric oscillators in monolithic mini-cavities. We show the tunability of the conical emission angle, the switching between different resonant cones, and simultaneous emission on different cones, depending on the pump angle as well as on the length of the resonator.

© 2005 Elsevier B.V. All rights reserved.

PACS: 42.65.Yj; 42.65.Sf; 47.54.+r

Transverse pattern formation in broad aperture lasers and in other nonlinear optical resonators like photorefractive oscillators, and optical parametric oscillators (OPOs) is attracting an increasing interest. The interest stems both: from the fundamental physical viewpoint, since the nonlinear optical systems are convenient systems for

studies of self-organization and pattern formation in spatially extended systems; from the viewpoint of applications, since optical patterns have an application potential for parallel information processing, for image processing, nonlinear microscopy, and related topics. Pattern formation in nonlinear *micro-* and *mini-cavities* is especially attractive from the application viewpoint due to the compactness of the system.

Transverse patterns have been predicted to occur and observed in several different nonlinear

\* Corresponding author. Tel.: +370 52698717; fax: +370 52366006.

E-mail address: [martynas.peckus@ff.vu.lt](mailto:martynas.peckus@ff.vu.lt) (M. Peckus).

optical systems (see, e.g. [1,2] for a review). In the case of a quadratic nonlinear interaction patterns have been predicted in OPOs [3–5], in degenerate OPOs [6–8], and in second harmonic generation (SHG) [9–11]. Degenerate OPOs are particularly interesting due to the possibility of excitation of phase patterns [12–14], and of phase solitons [15]. Experimentally transverse patterns have been observed for OPOs [16–18], and for second harmonic generation [19]. No patterns have been seen for *degenerate* OPOs, or for OPOs in monolithic cavities.

The work reported in the present article is a step towards spatial pattern generation in degenerate OPOs: we show the linear and weakly-nonlinear stage of the pattern formation, i.e., the conical (off-axis) emission. It is known that conical emission is an essential ingredient of transverse pattern formation: the patterns occur due to the instability of a homogeneous (trivial – dark or nontrivial – bright) solution with respect to spatially modulated modes with the modulus of transverse wave-number  $|k|$  depending on the resonator detuning. This means an off-axis (conical) emission with the cone angle depending on the detuning, which is a “weakly nonlinear” precursor of the nonlinear transverse patterns. In particular we show: (1) that the angle of conical emission is tunable; (2) that the emission on different resonant cones is possible; and (3) that the signal and idler waves can reside on different cones of resonance (multiconical emission). We also give a theoretical interpretation of the experimental observations.

The experiments used a BBO type I crystal of size  $5 \times 5 \times 1.7$  mm, with the thickness 1.7 mm along the

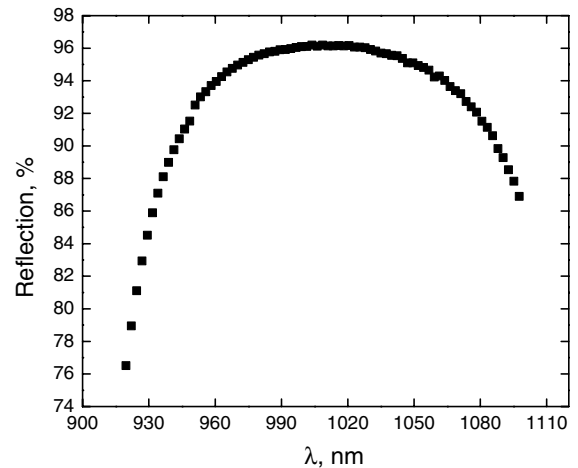


Fig. 1. Spectral characteristics of the coatings of the monolithic OPO mini-cavity.

propagation direction. The phase matching direction for degenerate parametric down conversion at 532 nm is coincident with the optical axis of the cavity (crystal orientation angles are:  $\theta = 22.8^\circ$ , and  $\phi = 90^\circ$ ). High-transmission coatings for 532 nm and high-reflection coatings for 1064 nm were used, resulting in a monolithic mini-cavity for subharmonic radiation. Fig. 1 shows experimentally recorded spectral characteristics of micro-cavity coatings for 1064 nm wave region. High reflectivity 94% at 1064 nm results in finesse of the cavity  $F = 50$ . Spectral measurements show that degenerate operation at 1064 nm occurs, resulting in a higher threshold for nondegenerate operation.

The experimental scheme is shown in Fig. 2. The pump source is a Nd:YAG passively modulated laser, generating 1064 nm pulses of 13 ns duration,

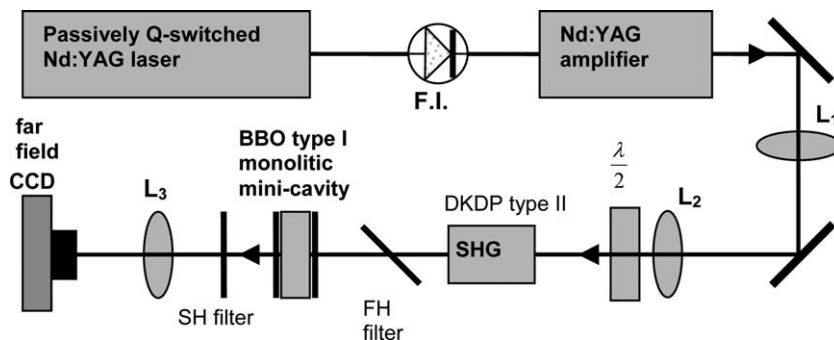


Fig. 2. Experimental scheme: F.I. – Faraday isolator;  $L_1$ ,  $L_2$  – telescope lenses;  $L_3$  – far field imaging lens.

5 mJ energy and TEM<sub>00</sub> spatial mode. A Nd:YAG double pass amplifier enhances the energy of the pulses up to 50 mJ. The diameter of the beam is  $\sim 2$  mm after reduction by a two lens telescope. The OPO pumping is performed by the second harmonic of the pump laser, generated in a DKDP type II crystal. A  $\lambda/2$  wave plate is used for energy attenuation of the pump beam. After second harmonic generation the fundamental frequency is completely filtered, so no seed injection was present in the experiments. In the case of 13 ns pulse duration, around 1000 resonant wave cavity round trips is possible in a 1.7 mm long BBO resonator. Q-switching of the pump laser leads to emission with a small number of longitudinal modes (usually a single- or two neighboring longitudinal modes are emitted). The mini-cavity orientation with respect to the pump beam can be changed in both directions. After passing the mini-cavity the pump beam is filtered out. A CCD camera and  $f$ - $f$  lens system was used for observation and recording of the OPO far field pattern.

First, we measured the main resonator characteristics of the mini-cavity. We explored the transmission of the cold resonator by illuminating it with radiation at the sub-harmonic at  $\lambda = 1064$  nm in the absence of a pump beam. Transmission resonances were observed at some angles as shown in

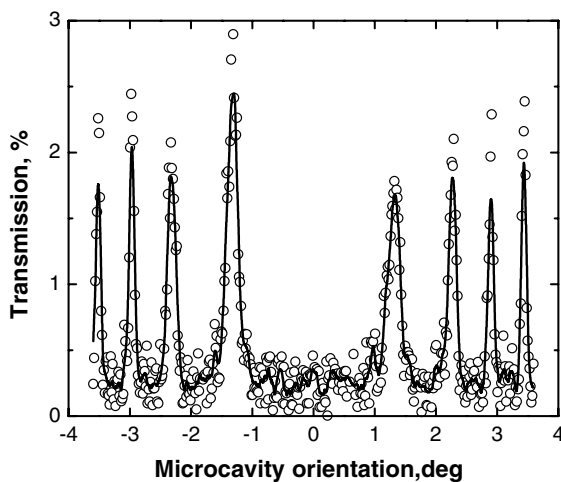


Fig. 3. Resonances of the cold cavity: an experimentally recorded transmission coefficient depending on a tilt of the cavity in one (of two possible) direction (continuous line – adjacent averaging smoothing of experimental points).

Fig. 3. The good separation of longitudinal modes (resonant rings) indicates relatively good finesse of the Fabry–Perot resonator, and certifies the above-evaluated value of resonator finesse. An additional variation of the detuning (the cavity length) is possible by changing the temperature of the monolithic mini-cavity, resulting in variation of the radii of the concentric rings. Temperature change over  $10^\circ\text{C}$  corresponds to the change of the full cavity length by one  $\lambda$ , i.e., allows tuning over a free spectral range of the mini-cavity transmission.

In the case of a monolithic BBO mini-cavity only a few parameters can be varied for achieving optical parametrical oscillation: (1) cavity face plate orientation with respect to the direction of the pump beam in both directions: along the phase matching direction and transversally to it and (2) cavity detuning through temperature induced crystal length change. In this experiment, we kept the cavity temperature constant. The BBO monolithic mini-cavity was pumped with 532 nm pulses of 10 mJ energy, and 13 ns duration. The pump beam diameter at the mini-cavity face plate was 2 mm. OPO radiation was observed for mini-cavity optical axes oriented at small  $0.5$ – $1.2^\circ$  angles with respect to the pump beam in the phase matching direction. The lowest OPO threshold of 7 mJ pump beam intensity ( $17\text{ MW/cm}^2$ ) was observed for  $0.75^\circ$  incidence angle (OPO conversion efficiency to signal and idler waves for a 10 mJ pump beam was 2.5%). Fig. 4 shows a typical far field OPO emission pattern. Signal and idler waves are

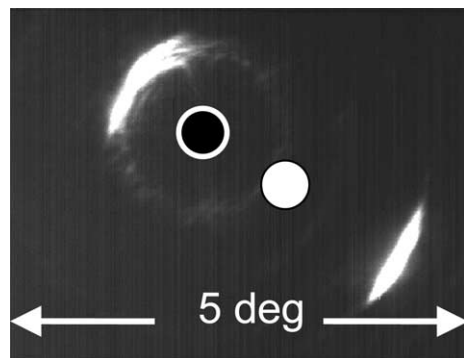


Fig. 4. Typical far field pattern of mini-cavity OPO emission. The empty spot indicates the direction of the mini-cavity optical axis, while the white spot indicates the direction of the pump.

always generated with a particular angle between them (conical emission). The pump beam direction is always between the signal and idler waves. In this picture, a faint pattern of cold cavity rings can also be observed.

The directions of the signal and idler waves and the angle of conical emission depend strongly on the mini-cavity orientation with respect to the pump beam as shown in Fig. 5(a)–(d). Fig. 5(a) shows the generation on one resonant cone; Fig. 5(b) indicates that two cone emission is possible. This generation pattern is very sensitive to cavity orientation in the phase matching direction, and is very weakly dependent on the pump energy, which indicates that the regime is quasi-linear.

When the mini-cavity orientation is changed in the nonphase matching direction, then the signal and idler waves rotate around the direction of the pump beam (Fig. 5(e)–(h)). Here, the mini-cavity orientation angle in the phase matching direction is fixed at a  $0.75^\circ$  angle. Our observations show that the signal and idler waves rotate around the pump beam direction by nearly  $180^\circ$  when the orientation is changed by  $\pm 1^\circ$ . The OPO threshold increases when the mini-cavity orientation in the nonphase matching direction exceeds  $0.5^\circ$ . At the value of  $1^\circ$  the OPO threshold energy rises from 7 to 15 mJ ( $36 \text{ MW/cm}^2$ ).

For a theoretical interpretation of the observed conical and multiconical patterns, we first describe

the formation of the ring structure of the far field in the cold cavity. We assume that the OPO radiation resides on the resonant rings of the cavity in accordance with the theory of multiconical OPO emission in monolithic resonators [20], and based on this assumption we describe the formation of OPO patterns.

As far as the resonant rings of the cold cavity is concerned, we recall that the intensity transmission coefficient of the Frabry–Perot cavity is given by

$$T = \frac{t_1 t_2}{1 + r_1 r_2 - 2\sqrt{r_1 r_2} \cos(\varphi)}, \quad (1)$$

where  $r_{1,2}$  and  $t_{1,2}$  are the reflection and transmission coefficients of the mirrors, calculated for the field amplitude (the intensity reflection and transmission coefficients are  $R_i = r_i^2$ ,  $T_i = t_i^2$  and  $R_i + T_i = 1$ ). The resonator finesse is related with the cavity parameters via a standard definition  $F = \pi(R_1 R_2)^{1/4} / (1 - \sqrt{R_1 R_2})$ , which in the limit of good cavity simplifies to  $F \approx 2\pi / (T_1 + T_2)$ . The  $\varphi$  is the phase shift over full resonator roundtrip of a wave tilted at the angle  $\alpha$  with respect to the optical axis of the cavity:  $\varphi = (l \cos(\alpha) - l_0) \cdot 2\pi / \lambda$ .  $l$  is the full length of the cavity,  $l_0$  is the full resonant length of the cavity, and  $\lambda$  is the wavelength. Eq. (1) results in a well-known ring structure (Fresnel rings) of the large aspect ratio resonators. Fig. 6 shows the ring structure as following from (1), and taking into account parameters of the cavity used in experiments:

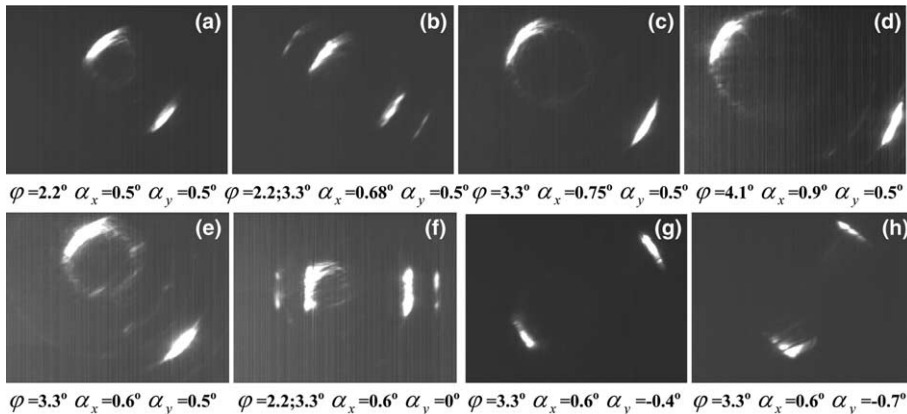


Fig. 5. Experimentally recorded far field pattern of DOPO. (a)–(d) Mini-cavity orientation as the pump beam is tilted in the phase-matching direction ( $\alpha_x$ ). (e)–(h) In the nonphase-matching direction  $\alpha_y$ .

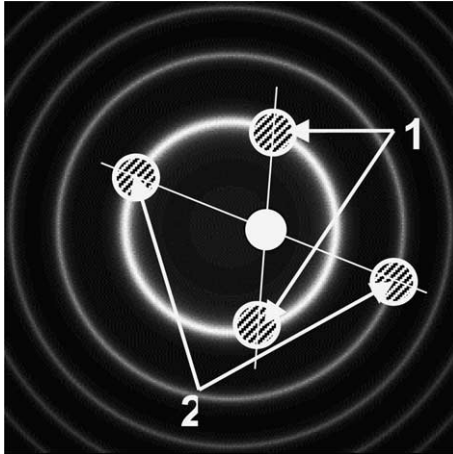


Fig. 6. Ring structure of a cold cavity. The white spot indicates direction of the pump beam, and the pairs of symmetrically (with respect to the pump direction) placed pattern spots illustrate possible directions of the OPO generation. The pair 1 illustrates OPO generation on the same (first) ring, the pair 2 – on two different rings. The ring density is inversely proportional to the full cavity length, and the radius of the inner ring depends on the off-resonance detuning.

we use the value of the full cavity length  $l$  in (1) as directly taken from experiments, and we choose the resonant cavity length  $l_0$  by matching the radii of the inner resonant ring in experimental observations and in numerical calculations. The rough interpretation of the experimentally observed patterns is illustrated in Fig. 6. We fix, for simplicity the origin of the coordinate system with the direction of the optical axis of the resonator, but vary the angle of the pump  $\alpha_0 = (\alpha_{0,x}, \alpha_{0,y})$  in both  $x$ , and  $y$ , directions, which correspond to the direction along and transversally to the direction of phase matching.

The OPO emission is determined essentially by the following three conditions:

1. By the resonance conditions for the mini-resonators (multicones with respect to the optical axis of the resonator) as described by (1), which means that the emission should reside on the resonant rings.
2. By the phase momentum conservation condition, which means that the emission in the far field domain must be symmetric with respect to the direction of the pump.
3. By the phase matching condition.

The pattern spots, as shown in Fig. 6, indicate the direction of OPO generation. It is obvious from this illustration that the fulfilment of the above conditions results in a complicated angular structure of the OPO generation.

Mathematically, the total gain of the OPO in the linear regime is given by

$$g(\alpha_{1,2}) = -\frac{\beta_1(\alpha_1) + \beta_2(\alpha_2)}{2} + \sqrt{\gamma(\alpha_{1,2})^2 + \frac{(\beta_1(\alpha_1) - \beta_2(\alpha_2))^2}{2}}, \quad (2)$$

as easily obtained from solution of equations describing parametric gain in lossy media (see, e.g. [21]). Here,  $\beta_{1,2}(\alpha_{1,2})$  are the coefficients of the losses for both generated waves depending on their angles (corresponding to the resonant ring structure – see condition 1), and  $\gamma(\alpha_{1,2})$  is the gain coefficient, which is dependent on the angles of both generated waves (the cone of phase matching in the case of vectorial synchronism – see condition 3). For a strong gain,  $\gamma \gg \beta_{1,2}$  (2) simplifies to  $g(\alpha_{1,2}) = \gamma(\alpha_{1,2}) - (\beta_1(\alpha_1) + \beta_2(\alpha_2))/2$ . The coefficients of losses follow directly from (1). Next, we take into account the momentum conservation condition with respect to the direction of pump beam. If we assume that the pump beam is a plane wave (spatial  $\delta$  – function in the far field domain) then the emission angles of both waves  $\alpha_{1,2}$  fulfil:  $\alpha_1 + \alpha_2 = 2\alpha_0$ . This allows to eliminate one angle (say  $\alpha_2$ ) from (2). Finally, introducing (e.g., phenomenologically) the expression of the phase matching  $\gamma(\alpha_{1,2})$  one obtains an analytical expression for the direction of the OPO generation  $\alpha_1$ . The resulting analytical expression for the angular distribution of OPO radiation in the far field is cumbersome, and we do not give it here. Instead, we plot the intensity distributions predicted by the formula in Fig. 7.

Qualitatively, the correspondence between experimentally observed (Fig. 5) and numerically obtained (Fig. 7) distributions is good. The conical emission angle varies with the angle of the pump by varying the pump angle in the phase matching direction (by varying the phase matching cone an-

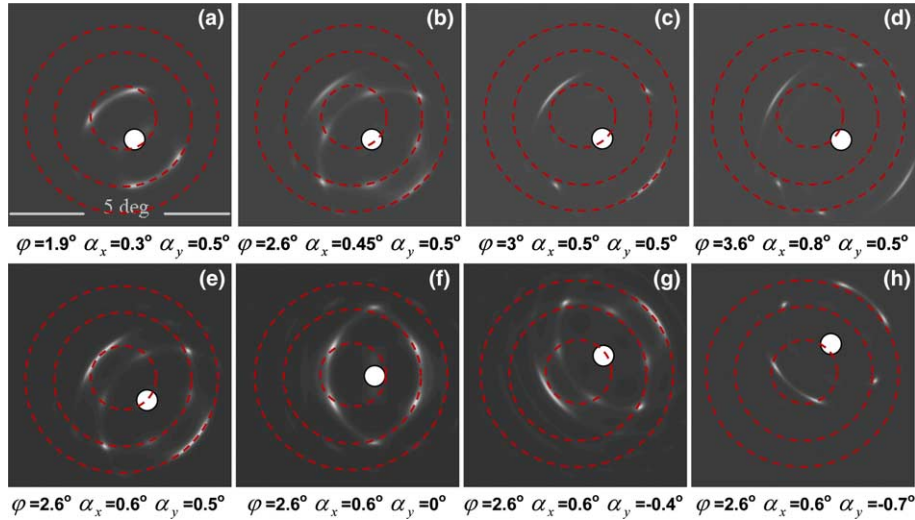


Fig. 7. Simulated OPO far field pattern. Resonator detuning  $\Delta = 0.2$  (as normalized to free spectral range), finesse  $F = 50$ , gain  $\gamma = 5$  (as calculated for to photon propagation length in a cold cavity),  $\varphi$  – the phase matching angle of OPO emission;  $\alpha_x$  – angle between coupling beam and cavity optical axes in phase matching direction,  $\alpha_y$  – angle in nonphase matching direction. Dashed concentric rings indicate the resonance rings of the cold cavity.

gle phenomenologically) as shown in Fig. 7(a)–(d). Also the far field patterns rotate by varying the pump angle in the direction perpendicular to the phase matching direction, as shown in Fig. 7(e)–(h). Typically, upon varying the pump angle, the radial and the azimuthal emission angles vary smoothly, before they jump abruptly to new locations. The quantitative correspondence between the far field distributions for different angles between the pump wave and the optical axis of the resonator is also good.

In conclusion, we demonstrated OPO generation in a monolithic BBO type I crystal mini-cavity. We show that OPO emission in a monolithic mini-cavity is conical and multiconical, so signal and idler wave directions depend on cavity detuning to laser frequency, phase matching cone and cavity orientation with respect to the pump beam. This allows the OPO emission direction to be controlled by changing the mini-cavity orientation, by temperature changes or by laser frequency change. In the case of external monolithic mini-cavity refractive index change, or external phase matching condition change, the OPO emission angles can be modulated or attenuated (external electric field or external light induced refractive index change).

We expect that OPO far field control is also possible for a nonmonolithic cavity, although the monolithic mini-cavity is attractive for compactness and stability of the cavity alignment.

### Acknowledgements

Financial support from NATO Linkage Grant PST.CGL.979050 and Lithuanian State Science and Studies Foundation is acknowledged. M.S. was supported by National Science Foundation Grant ECS-0200372, and K.S. by Project FIS2004-02587 of the Spanish Ministry of Science and Technology.

### References

- [1] L.A. Lugiato, M. Brambilla, A. Gatti, *Adv. Atom. Mol. Opt. Phys.* 440 (1998) 229.
- [2] K. Staliunas, V.J. Sanchez-Morcillo, *Transverse Patterns in Nonlinear Optical Resonators* Springer Tracts in Modern Physics, vol. 183, Springer, Berlin, 2003.
- [3] K. Staliunas, *Opt. Commun.* 90 (1992) 82.
- [4] G.-L. Oppo, M. Brambilla, D. Camesasca, A. Gattiand, L.A. Lugiato, *J. Mod. Opt.* 41 (1994) 1151.

- [5] S. Longhi, A. Geraci, *Phys. Rev. A* 54 (1996) 4581.
- [6] K. Staliunas, *J. Mod. Opt.* 42 (1995) 1261.
- [7] G.J. de Valcarcel, K. Staliunas, Eugenio Roldán, V.J. Sánchez-Morcillo, *Phys. Rev. A* 54 (1996) 1609.
- [8] M. Tlidi, P. Mandel, M. Haelterman, *Phys. Rev. E* 56 (1997) 6524.
- [9] C. Etrich, U. Peschel, F. Lederer, *Phys. Rev. Lett.* 79 (1997) 2454.
- [10] C. Etrich, U. Peschel, F. Lederer, *Phys. Rev. E* 56 (1997) 4803.
- [11] P. Lodahl, M. Saffman, *Phys. Rev. A* 60 (1999) 3251.
- [12] S. Trillo, M. Haelterman, A. Sheppard, *Opt. Lett.* 22 (1997) 970.
- [13] K. Staliunas, V.J. Sanchez-Morcillo, *Phys. Lett. A* 241 (1998) 28.
- [14] M. Tlidi, P. Mandel, *Phys. Rev. Lett.* 81 (1998) 979.
- [15] K. Staliunas, V.J. Sanchez-Morcillo, *Phys. Rev. A* 57 (1998) 1454.
- [16] V. Sirutkaitis, R. Grigonis, G. Sleky, K. Staliunas, *Quantum Semicl. Opt.* 1 (1999) 139.
- [17] M. Vaupel, A. Maître, C. Fabre, *Phys. Rev. Lett.* 83 (1999) 5278.
- [18] S. Ducci, N. Treps, A. Maître, C. Fabre, *Phys. Rev. A* 64 (2001) 023803.
- [19] A.V. Mamaev, P. Lodahl, M. Saffman, *Opt. Lett.* 28 (2003) 31.
- [20] S. Longhi, *Opt. Commun.* 153 (1998) 90.
- [21] L.A. Lugiato, C. Oldano, C. Fabre, E. Giacobino, R. Horowicz, *Nuovo Cimento D* 10 (1988) 959.